Theoretical and Experimental Studies of Polymer Adsorption and Polymer Mediated Interactions

Xie, Fei

2016

Document Version:
Publisher's PDF, also known as Version of record

Theoretical and Experimental Studies of Polymer Adsorption and Polymer Mediated Interactions

Theoretical and Experimental Studies of Polymer Adsorption and Polymer Mediated Interactions

Fei Xie

Division of Theoretical Chemistry
Lund University, Sweden

LUND
UNIVERSITY

Thesis for the degree of Doctor of Philosophy
Faculty opponent: Frans Leermakers, Wageningen University

To be presented, with the permission of Lund University, this thesis will be publicly defended in lecture hall B at the Center for Chemistry and Chemical Engineering (Kemicentrum) on Friday, the 22nd of April 2016 at 10:30.

Organization	Document name
LUND UNIVERSITY Division of Theoretical Chemistry Box 124 SE–221 00 LUND Sweden	**DOCTORAL DISSERTATION** Date of disputation 2016-04-22 Sponsoring organization Swedish Research Council
Author(s) Fei Xie	

Title and subtitle

Theoretical and Experimental Studies of Polymer Adsorption and Polymer Mediated Interactions

Abstract

Polyelectrolyte adsorption and polymer mediated interactions in different colloidal polymer systems have been studied in this work. Theoretical methods and experimental techniques are combined, in order to obtain more general reliable results, as well as a deep understanding of the molecular mechanisms that are responsible for the observed behaviors. Two different types of highly charged cationic polyions have been used to explore the adsorption onto oppositely charged surfaces. The adsorption varies with concentration of simple salt and the adsorption dependence on molecular weight have been considered. Polymer density functional theory and null ellipsometry have been utilized to study the adsorption. Various colloidal polymer systems have also been investigated in order to scrutinize polymer mediated interactions. For systems containing charged colloidal particles and non-adsorbing polyethylene oxide (PEO) chains, we studied gelation and constructed a coarse-grained model, to quantitatively compare predicted structure factors with corresponding experimental data. We have devoted some extra efforts to predict and understand the temperature response of polymer mediated interactions, in systems where the pure polymer solution display an local critical solution temperature (LCST). This has, for instance, resulted in predictions that such colloidal particle + polymer dispersions can display a phase behavior that responds on a non-monotonic manner to temperature change (specifically: flocculated - dispersed - flocculated). these predictions are in qualitative agreement with experiments, and achieved without any assumptions of temperature-dependent interactions. Another prediction from our studies on LCST polymer solutions, is that these may undergo phase separations in porous environments, even though there is only one phase for all compositions in the bulk solution.

Key words

Polyelectrolyte, Adsorption, Colloid, Polymer, Dispersion, Interaction, Ellipsometry, Monte Carlo Simulations, Classical Density Functional Theory.

Classification system and/or index terms (if any)

Supplementary bibliographical information	Language
	English
ISSN and key title	ISBN
	978-91-7422-434-4
Recipient's notes	Number of pages: 180 / Price
	Security classification

Theoretical and Experimental Studies of Polymer Adsorption and Polymer Mediated Interactions

Fei Xie

Division of Theoretical Chemistry
Lund University, Sweden

LUND
UNIVERSITY

Cover illustration front: Part of density functional theory code, decorated with spring leaves.

Funding information: This work was financially supported by Swedish Research Council.

Center for Chemistry and Chemical Engineering
Division of Theoretical Chemistry
ISBN: 978-91-7422-434-4

Printed in Sweden by Media-Tryck, Lund University, Lund 2016

Contents

List of publications

I **Polyelectrolyte adsorption on solid surfaces: theoretical predictions and experimental measurements.**

F. Xie., T. Nylander., L. Piculell., S. Utsel., L. Wågberg., T. , Åkesson and J. Forsman.
Langmuir, 2013, 29(40), pp. 12421–12431.

II **Theoretical and experimental investigations of molecular weight dependence on polyelectrolytes adsorption**

F. Xie., H. Lu., T. Nylander., L. Wågberg. and J. Forsman.
Submitted to *Langmuir*, 2016.1.

III **Fluid-fluid transitions at bulk supercritical conditions.**

F. Xie., C. E. Woodward., and J. Forsman.
Langmuir, 2013, 29(8), pp 2659–2666.

IV **Non-monotonic temperature response of polymer mediated interactions.**

F. Xie., C. E. Woodward., and J. Forsman.
Soft matter, 2016, 12, pp 685-663.

V **Theoretical Predictions of Temperature-Induced Gelation in Aqueous Dispersions Containing PEO-Grafted Particles**

F. Xie., C. E. Woodward., and J. Forsman.
Submitted to *J. Phys. Chem. B*, 2016.2.

VI **A simple and versatile implicit solvent model for Polyethylene Glycol in aqueous solution at room temperature.**

F. Xie., M. Turesson.; M. Jansson.; M. Skepö.; and J. Forsman.
Polymer, 2016, 84, pp 132-137.

VII **Theoretical predictions of structures in dispersions containing charged colloidal particles and non-adsorbing polymers..**

F. Xie., M. Turesson., C. E. Woodward., K. van Gruijthuijsen., A. Stradner., and J. Forsman.
Submited to *PCCP*, 2016.1.

All papers are reproduced with permission of their respective publishers.

Acknowledgements

To start my PhD in theoretical chemistry of Lund University is definitely one of the best decisions I have ever made in my life. I am so fortunate to have **Jan Forsman**, who is an excellent scientist, also a brilliant photographer, as my main supervisor. **Janne**, thanks for being patient, and supportive all the time. You introduced this fantastic theoretical world to me, and always have the magic to make the complicated theory and calculations easy to understand, and fun to learn! In my opinion, your brain is like a calculator, it is amazing that you are so efficient every time. I will always remember 'janne's rule', which is: 'It should be fast, and it should be correct!'. Anyway, it has been so delightful to work with you all these years, not only the scientific work, but also the daily pleasant chat. Thanks for your inspirations and encouragements on my Swedish as well, 'Det går fler tåg', makes me always remember to look at the positive side if something bad happens.

I would like to thank **Tommy Nylander**, my supervisor on experimental part. You are always there to help me whenever I need you, e.g., help me to sort out experimental problems, rehearse my presentations, give advice on my manuscript and thesis writing. Thanks for all your useful suggestions and professional advice. You are always enthusiastic and it is so joyful to talk with you every time. Thanks **Lennart Piculell**, my cosupervisor, you are like a professional Chemistry resource for me, I can always get scientific help from you. Thanks **Mikael Lund** for all the technique supports. Things would not go so smoothly without your help. Thanks **Marie Skepö** for the lab work help, and for taking me to Grenoble, so I had chance to see the impressive synchrotron radiation facility, and experience the very nice French cuisine. Thanks **Clifford Woodward** for all the valuable collaborations.

Thanks to our administrator **Helena Persson** for helping me with all the documentation stuff, and engineer **Maria Södergren** for helping me purchase experimental materials, and look after us in the lab. Special thanks to dearest **Ingrid G Nilsson**, for helping me settle up when I just came to Sweden, and took good care of us. Enjoy your retirement, and I will always miss you! Thanks **Paula Leckius**, for your professional skills on scientific printing of my thesis!

I would like to thank **Wuge Briscoe**, supervisor of my master study in Bristol University, for introducing this wonderful country (Sweden) and excellent University to me. It always right to follow your advice :). I also would like to mention my uncle **Luting Ma**, who is an outstanding educationist, and my cousin **Jie Ma**, who is a brilliant Chemist. Thank you for offering me the chance to study aboard when I was just an undergraduate and confused about the future. You encouraged me to be brave and independent, gave me vital support and help. Those mean a lot to me.

Thanks to all my friend and colleagues, you make my life sunny even in the long Swedish dark winter time. Thanks **Ryan**, **Hongduo**, **Ruiyu**, **Dat**, **Anil** and **Martin Trulsson**, for cheering me up and spreading joy around me. Special thanks to **Martin Trulsson**, for helping me go through my thesis, spotting errors and giving useful suggestions.

Thank you very much my dear parents, for your endless support and unconditional love. And **Zhecheng**, I am so lucky to have met you and married you, thank you for looking after me and spoiling me. I love you, always and forever.

Popular Scientific Summary

Milk, clay, ink and paint are examples of colloidal dispersions. These all contain particles with a diameter in the range from about 10 nanometers to about 1 micrometer. Unless they are charged, such particles have a tendency to attract, and this attraction may cause them to flocculate/precipitate. A process by which the particles are pushed further away from each other is called a "stabilizing" process, while the opposite is de-stabilizing. Both processes are utilized industrially as well as in biological systems.

Polymers are chain-like molecules that, in the simplest case, are composed of many identical repeating units. The latter are called monomers. Interestingly enough, one can often utilize polymers to either stabilize or de-stabilize colloidal dispersions. The outcome depends on the way in which the polymers mediate interaction between the particles, and what makes polymers special is that these forces can be mediated by the molecules themselves!

In our work, we have attempted to unravel underlying molecular mechanisms for such processes, as well as the related phenomenon of polymers adsorbing at surfaces. In some systems, the monomers that build up the polymers are charged. The combination of such charged polyions, and the free and oppositely charged counterions, is called a "polyelectrolyte." The way in which polymers adsorb and mediate particle interactions generally change with conditions, such as pH (how acidic the solution is), temperature, polymer length etc. We have devoted combined experimental and theoretical efforts to investigate these phenomena, and hopefully our work has contributed to the understanding of such processes.

Chapter 1

Polymer Mediated and Electrostatic Interactions

In this chapter, important polymer mediated interactions, as well as electrostatic interactions between surfaces in aqueous solutions are summarized.

1 Polymer Mediated Interactions

1.1 Polymers and Colloidal Dispersions

Commonly occurring interactions between polymer and surfaces in aqueous solutions are introduced in this section.

Polymers

A polymer, is a macromolecule which contains large number of repeated segments. Those segments are also called monomers. Polymers can be divided into two categories, homopolymers and copolymers, where the former carries identical repeating units. The architecture of polymers, such as simple linear chains or branched polymers, can affect many physical properties of corresponding solutions and melts. Various techniques can be applied to the synthesis process of polymers with a range of architectures, chain lengths and polydispersities.

When polymers are dissolved in a solutions, their average conformations depend on the solvent properties. In a poor solvent, the polymer chains are usually in a globule

state, while in theta solvent, they behave as random coils. In good solvents, expanded coils of polymer chains are expected.

As the polymer usually contains chains with unequal lengths, the polymer molecular weight usually displays a distribution rather than a single value. Therefore, it is necessary to calculate the average molecular weight from all the polymer chains. Two commonly used averages are the number averaged molecular weight M_n and weight averaged molecular weight M_w. M_n describes the statistical average molecular weight of all the polymer chains in a sample. It is defined as:

$$\langle M_n \rangle = \frac{\sum N_i M_i}{\sum N_i} \tag{1.1}$$

where M_i is the molecular weight of a chain, N_i is the number of chains of that molecular weight.

M_w considers the contribution from the molecular weight of a chain to the molecular weight average. It is defined as:

$$\langle M_w \rangle = \frac{\sum N_i M_i^2}{\sum N_i M_i} \tag{1.2}$$

The ratio between M_w and M_n, is called the Polydispersity index (PDI). It is often used to determine the polydispersity of polymers, *i.e.* the width of the molecular weight distribution. A PDI value closes to 1 indicates a more narrow molecular weight distribution [6].

Colloidal Dispersions

A colloidal dispersion is a heterogeneous system which contains particle sizes ranging between 1 and 1000 nm in diameter. Aqueous colloidal dispersions are widely applied in food products and other materials, for example paint, ink and coatings. Adding polymers to a colloidal dispersion can stabilize the system, or lead to phase transition and aggregation, depending on the conditions, such as polymer concentration, pH value, temperature and so on.

1.2 Steric or Overlap Interactions

Polymers can be grafted onto surfaces, thus forming polymer-covered surfaces. When two such surfaces approach, the surfaces may experience a repulsion when the polymer

layers start to overlap. This will typically happen in a good solvent. The reason is the unfavorable entropy loss resulting from a compression of the polymer chains between surfaces. This kind of repulsion is referred to 'steric or overlap repulsion', see Figure 1.1. This interaction is normally sufficient to stabilize the colloidal dispersions, and as therefore called 'steric stabilization'.

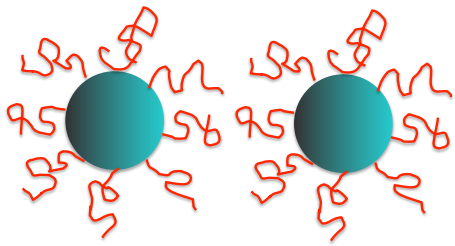

Figure 1.1: Sketch of steric stabilization in colloidal dispersion.

1.3 Depletion Interactions

In a colloidal polymer dispersion, if the monomers are repelled from the particle surfaces, the polymers tend to stay far from the surfaces in order to avoid entropy loss. Thus the polymers can efficiently push the surfaces together by osmosis, since the polymer concentration is low in interparticle regimes. This mechanism is called depletion attraction (Figure 1.2). Some small solute molecules, such as polymers, micelles and so on, which are non-adsorbing to particle surfaces, can be used as depletants. Adding depletants into colloidal dispersions can generate depletion attractions, which find a wide range of applications in aggregating fragile biological or colloidal structures.

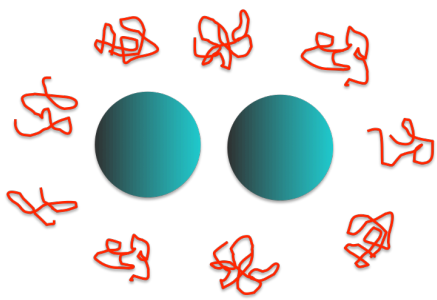

Figure 1.2: Sketch of depletion attractions between colloidal particles in the presence of non-adsorbing polymers.

1.4 Bridging Interactions

Another type of attractive polymer mediated interaction is associated with polymers which have tendency to adsorb on the surfaces. When two such polymer coated surfaces approach each other, attractive interactions are generated between the polymers and the opposite surfaces. Polymers then behave like a 'bridge' between the two surfaces, which explains the name 'bridging interaction' (Figure 1.3) . This interaction is very common in both biological and non-biological colloidal systems.

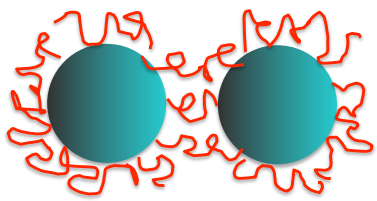

Figure 1.3: Sketch of bridging interactions between two polymer-coated colloidal particles.

2 Electrostatic Interactions

2.1 Coulomb Interaction

The Coulomb interaction describes the interaction free energy between two charges (Q_1 and Q_2). In vacuum, the energy $u(r)$ is given by:

$$u(r) = \frac{Q_1 Q_2}{4\pi\varepsilon_0 r} = \frac{z_1 z_2 e^2}{4\pi\varepsilon_0 r} \tag{1.3}$$

where ε_0 is the vacuum permittivity, with a value of $8.854 \times 10^{-12} C^2 J^{-1} m^{-1}$, z_1 and z_2 are the ionic valencies, e is the elementary charge ($e = 1.602 \times 10^{-19} C$), and r is the separation between the two charges. For similarly charged ions, the Coulomb force is repulsive and interaction is positive, but if the valencies have different signs, the Coulomb interaction is attractive.

Let us also consider the potential of mean force (PMF) between two charges Q_1 and Q_2 in a solvent. If we put those two charges in water, the solvent molecules will almost cancel out the original electric field. With fixed r, the PMF can be written as:

$$\beta w(r) = -\ln[\frac{\int \exp(-\beta U_{tot}(\mathbf{R}^N, r)) d\mathbf{R}^N}{\int d\mathbf{R}^N}] \tag{1.4}$$

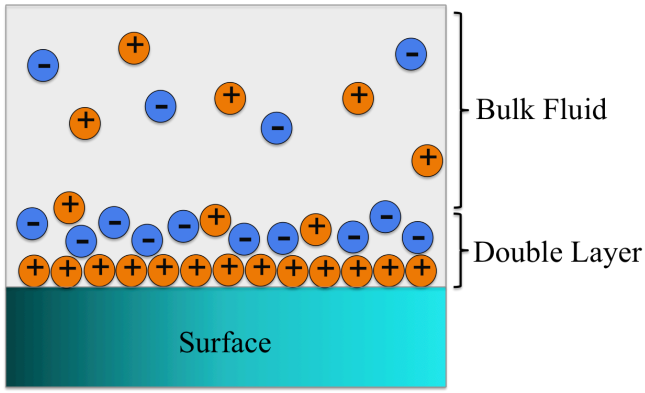

Figure 1.4: Sketch of electric double layer.

where β is the inverse thermal energy, $\mathbf{R}^N$ denotes the N solvent molecules, and U_{tot} is the total interaction energy of the system. It turns out that this complicated integral can be approximated by the remarkably simple expression (at large separations):

$$w(r) = \frac{Q_1 Q_2}{4\pi\varepsilon_0\varepsilon r} = \frac{z_1 z_2 e^2}{4\pi\varepsilon_0\varepsilon r} \tag{1.5}$$

where ε is the relative permittivity of the solvent. In other words, the overall influence to the ion-ion interaction from all the 'extra interactions' (relative to the gas phase) there are in the solvent, approximately amounts to a simple scale factor $1/\varepsilon$. Similar simplifying, albeit approximate, PMFs are commonly utilized in a coarse-grained models of polymer solutions.

2.2 The Electric Double Layer

The electric double layer describes the ionic structure near a charged surface immersed in a solution. The structure usually contains two charged layers. The first one is bonded to the surface by chemical interaction. The free ions in the solution will stay near the surface due to the Coulomb force, thus forming a second layer, which is more loosely associated with the surface than the first one. This second layer is also called 'the diffuse layer'.

2.3 The Poisson-Boltzmann (PB) Equation

The Possion equation in an electrolyte solution has the following form:

$$\varepsilon_0 \varepsilon_r \nabla^2 \Phi = -\rho \tag{1.6}$$

where ∇^2 is the Laplacian operator, ρ is the charge distribution, and $\mathbf{\Phi}$ is the electrostatic potential.

Noted that the ions in the electrolyte solution are free to move in response to the electrical field, according to Boltzmann distribution, the charge distribution can be expressed as:

$$\rho = e \sum_i z_i c_0 \exp(\frac{-z_i e \Phi}{kT}) \tag{1.7}$$

where z_i stands for the ion valency and c_0 is the bulk solution concentration, while k is the Boltzmann's constant. By combining Equation 1.6 and Equation 1.7, we obtain the Poisson-Boltzmann equation (Equation 1.9).

$$-\varepsilon_0 \varepsilon_r \nabla^2 \Phi = e \sum_i z_i c_0 \exp(\frac{-z_i e \Phi}{kT}) \tag{1.8}$$

The Poisson-Boltzmann equation is a non-linear second order differential equation. It can be used to describe the ion distribution in an electrolyte solution outside a charged surface. Further approximation can be made to linearize the function under low potential conditions.

$$-\varepsilon_0 \varepsilon_r \nabla^2 \Phi = e \sum_i z_i c_0 \exp(\frac{-z_i e \Phi}{kT}) = e \sum_i z_i c_0 - e \sum_i (\frac{z_i^2 c_0 e \Phi}{kT}) \tag{1.9}$$

Since $\sum_i z_i c_0 = 0$ due to electroneutrality of the system, we can obtain the linearized Poisson-Boltzmann equation (Equation 1.10), which is more simple and commonly used for a wide variety of cases.

$$\varepsilon_0 \varepsilon_r \nabla^2 \Phi = e \sum_i (\frac{z_i^2 c_0 e \Phi}{kT}) \tag{1.10}$$

2.4 Debye Length

Debye length, $(1/\kappa)$, which describes the range of electrostatic interactions in electrolyte solutions. It is given by:

$$\frac{1}{\kappa} = \left(\frac{\varepsilon_0 \varepsilon_r kT}{\sum_i (z_i e)^2 c_0}\right)^{1/2} \tag{I.II}$$

The Debye length decreases with increasing salt concentration, since the ions in the solution then more efficiently screen away the surface charges.

Chapter 2

Theoretical Tools

1 *Classical* Density Functional Theory (DFT)

Here, we present a *classical* density functional theory (DFT), which minimizes the free energy of the system as a functional of molecular densities. Thus, the equilibrium density profile, as well as the free energy, can be obtained. In systems where at least one dimension can be (approximately) integrated away, DFT is a fast, versatile method in comparison with Monte Carlo and Molecular dynamics simulations, and also feasible for realistic polymer lengths.

1.1 *Classical* Density Functional Theory

Let us start with a canonical ensemble (T, V, N), where T, V, N denote the fixed temperature, volume and number of particles in the system. For a homogeneous system containing N identical particles, the configurational partition function (Q_c) can be expressed as:

$$Q_c = \frac{1}{N!} \int e^{-\beta U(\mathbf{r}^N)} d\mathbf{r}^N \tag{2.1}$$

This function is very difficult to solve. However, we can simplify the system by assuming that the interactions are pairwise additive, and that the interactions are spherically symmetric. A rather drastic further simplification ensures if we also invoke a mean-field assumption, wherein all particle correlations are neglected. If we locate

a randomly chosen 'tagged' particle at the origin, the mean-field energy per particle, $e_p^{(MF)}$ can be written as:

$$e_p^{(MF)} = 2\pi \int_0^\infty nr^2 \phi(r) dr \tag{2.2}$$

where $\phi(r)$ is the pair potential, $n = N/V$ is the density and V is the total volume. The total mean-field interaction energy, $U^{(MF)}$, is then simply given by $U^{(MF)} = N \cdot e_p^{(MF)}$ and:

$$Q_c^{(MF)} = \frac{1}{N!} V^N e^{-\beta N 2\pi \int_0^\infty nr^2 \phi(r) dr} \tag{2.3}$$

As already mentioned, in the mean field energy expressions, we have neglected particles correlations. By introducing the radial distribution function, $g(r)$, we arrive at a more accurate expression for the energy per particle, e_p:

$$e_p = 2\pi \int_0^\infty nr^2 g(r) \phi(r) dr \tag{2.4}$$

If we consider the particles as hard spheres with diameter σ, and approximate $g(r)$ is a simple step function, where the step enters at a interparticle separation σ. The expression for the energy per particle then becomes:

$$e_p = 2\pi \int_\sigma^\infty nr^2 \phi(r) dr \tag{2.5}$$

This implies that a volume is excluded to the particles. The free volume, V_{free}, is defined in terms of the excluded volume per particle, v_0:

$$V_{free} = V - Nv_0 \tag{2.6}$$

The partition function can thus be written as:

$$Q_c = \frac{1}{N!} (V - Nv_0)^N e^{-\beta N 2\pi \int_\sigma^\infty nr^2 \phi(r) dr} \tag{2.7}$$

The Helmholtz' free energy, $\mathcal{F}$, is then given by:

$$\beta \mathcal{F} = -\ln Q_c = N \ln \frac{N}{V - Nv_0} - N + 2\pi \frac{N^2}{V} \beta \int_\sigma^\infty r^2 \phi(r) dr \tag{2.8}$$

For a heterogeneous system which has a non-uniform density distribution $n = n(\mathbf{r})$ and $N = \int n(\mathbf{r})d\mathbf{r}$, the Helmholtz' free energy can be expressed as a functional of the density distribution, with an external field (V_{ex}) included:

$$\begin{aligned}\beta\mathcal{F} = &\int n(\mathbf{r}) \ln[\frac{n(\mathbf{r})}{1 - n(\mathbf{r})v_0}] - n(\mathbf{r})d\mathbf{r} \\ &+\frac{\beta}{2}\int n(\mathbf{r}) \int' n(\mathbf{r}')\phi(\mid \mathbf{r} - \mathbf{r}' \mid)d\mathbf{r}'d\mathbf{r} \\ &-\beta \int V_{ex}(\mathbf{r})n(\mathbf{r})d\mathbf{r} \end{aligned} \tag{2.9}$$

where the prime on the integral indicates that the region $\mid \mathbf{r} - \mathbf{r}' \mid < \sigma$ should be excluded.

The grand potential (Ω) is:

$$\begin{aligned}\beta\Omega = \beta[\mathcal{F} - \int \mu n(\mathbf{r})d\mathbf{r}] = &\int n(\mathbf{r}) \ln \frac{n(\mathbf{r})}{1 - n(\mathbf{r})v_0} - n(\mathbf{r})d\mathbf{r} \\ &+\frac{\beta}{2}\int n(\mathbf{r}) \int' n(\mathbf{r}')\phi(\mid \mathbf{r} - \mathbf{r}' \mid)d\mathbf{r}'d\mathbf{r} \\ &-\beta \int (V_{ex}(\mathbf{r}) - \mu)n(\mathbf{r})d\mathbf{r} \end{aligned} \tag{2.10}$$

1.2 *Classical* Density Functional Theory for Polymers

The Theory

The DFT theory has been extended to 'Polymer DFT' by Woodward [35].

Consider a polymer composed of N_r monomers, modeled as q connected beads. Each monomer is made up of q/N_r connected beads, and a polymer configuration can be represented by $\mathbf{R} = (\mathbf{r}_1, ..., \mathbf{r}_q)$. Let $N(\mathbf{R})$ define a multipoint density distribution, where $N(\mathbf{R})d\mathbf{R}$ is the number of polymer molecules having configurations between $\mathbf{R}$ and $\mathbf{R} + d\mathbf{R}$. A bonding potential $V_b(\mathbf{R})$ is introduced since the beads are connected by bonds. The total free energy $\mathcal{F}$, is a sum of $\mathcal{F}_{id}$ and $\mathcal{F}_{ex}$, where $\mathcal{F}_{id}$ denote the ideal free energy functional of a solution containing ideal polymers, with no bead-bead interactions except for the connecting bonds, while $\mathcal{F}_{ex}$ denote the excess free energy. This accounts for the interparticle interactions, including excluded volume

terms (hard-sphere part) and long-range bead-bead interactions (the soft term). The ideal free energy term can be specifically expressed as Equation 2.11, with an external field V_{ex} acting on all the beads.

$$\beta\mathcal{F}_{(id)} = \int N(\mathbf{R})\left(\ln[N(\mathbf{R})] - 1\right) d\mathbf{R} + \beta \int N(\mathbf{R}) V_b(\mathbf{R}) d\mathbf{R} + \beta \int n_m(\mathbf{r}) V_{ex}(\mathbf{r}) d\mathbf{r} \tag{2.11}$$

Where $n_m(\mathbf{r})$ is the bead density, it is defined as:

$$n_m(\mathbf{r}) = \sum_{i=1}^{q} \int \delta(\mathbf{r} - \mathbf{r}_i) N(\mathbf{R}) d\mathbf{R} \tag{2.12}$$

Notice that the solution is in equilibrium with a bulk solution which has a chemical potential μ_p, so the grand potential, Ω, can be described as:

$$\Omega = \mathcal{F}_{id} - \mu_p \int N(\mathbf{R}) d\mathbf{R} \tag{2.13}$$

We can then minimize the free energy as a functional of the polymer density distribution, and establish the equilibrium monomer density profile ($N_{eq}(\mathbf{R})$):

$$N_{eq}(\mathbf{R}) = e^{\beta(\mu - V_{ex}(\mathbf{R}) - V_b(\mathbf{R}))} \tag{2.14}$$

If we have excess free energy $\mathcal{F}_{ex}$ included, we will also have:

$$\frac{\delta\mathcal{F}_{ex}(\mathbf{R})}{\delta N(\mathbf{R})} = \sum_{i=1}^{q} \frac{\delta\mathcal{F}_{ex}[n_i(\mathbf{r}_i)]}{\delta n_i(\mathbf{r}_i)} \tag{2.15}$$

Excluded Volume Considerations

We have considered two ways to estimate excluded volume effects in polymer DFT, namely, the Generalized Flory-dimer (GFD) method and the Locally Incompressible Fluid model (LIF).

Generalized Flory-Dimer (GFD) Equation of State

The GFD equation of state estimates the excluded volume of bonded monomer pairs by using an approximate equation of state for dimers. By implementing the GFD

equation of state in polymer DFT, we can approximate the entropy loss caused by excluded volume [35].

Incompressible Fluid Model (LIF)

In the LIF model, the polymer solution is considered as a locally incompressible system. Monomers and solvent particles are assumed to have equal size, and the total density (n_t) of monomer and solvent particles is constrained to a fixed value:

$$n_t = n_m(\mathbf{r}) + n_s(\mathbf{r}) \tag{2.16}$$

where $n_m(\mathbf{r})$ is the monomer density distribution, $n_s(\mathbf{r})$ is the solvent particle density distribution. The excess free energy caused by excluded volume can be expressed in term of the monomer density, which is related to the solvent density as well, noticed that $n_s(\mathbf{r}) = n_t - n_m(\mathbf{r})$. The excess free energy in LIF is given by:

$$\beta\mathcal{F}_{ex} = \int [n_t - n_m(\mathbf{r})] \ln[n_t - n_m(\mathbf{r})] - n_t + n_m(\mathbf{r}) d\mathbf{r} \tag{2.17}$$

1.3 DFT for Degenerate System

Here we introduce the DFT for degenerate systems. Assume that each monomer can be in either of two calsses of states, $'A'$ or $'B'$, where A monomers are solvophilic while B monomers are solvophobic. This model was first suggested by Karlström [16] for Polyethylene oxide (PEO) in aqueous solution. We can introduce the monomer state probabilities, P_A and P_B, then arrive at the following free energy functional $\mathcal{F}$:

$$\begin{aligned}
\beta\mathcal{F} \;=\; & \int N(\mathbf{R}) \left(\ln[N(\mathbf{R})] - 1\right) d\mathbf{R} + \beta \int N(\mathbf{R}) V_b(\mathbf{R}) d\mathbf{R} + \\
& \int [(n_t - n_m(\mathbf{r})) \ln [n_t - n_m(\mathbf{r})] + n_m(\mathbf{r})] d\mathbf{r} + \beta\mathcal{U}[n_m(\mathbf{r}), P_A(\mathbf{r})] + \\
& \int n_m(\mathbf{r})(1 - P_A(\mathbf{r})) \ln \left[\frac{1 - P_A(\mathbf{r})}{g_B}\right] d\mathbf{r} + \\
& \int n_m(\mathbf{r}) P_A(\mathbf{r}) \ln \left[\frac{P_A(\mathbf{r})}{g_A}\right] d\mathbf{r} + \\
& \beta \int [(n_m(\mathbf{r}) P_A(\mathbf{r}) V_{ex}^{(A)}(\mathbf{r}) + n_m(\mathbf{r})(1 - P_A((\mathbf{r})) V_{ex}^{(B)}(\mathbf{r}) + \\
& (n_t - n_m(\mathbf{r})) V_{ex}^{(s)}(\mathbf{r}))] d\mathbf{r}
\end{aligned} \tag{2.18}$$

where $\mathcal{U}[n_m(\mathbf{r}), P_A(\mathbf{r})]$ is the attractive interparticle interactions.

In our work, this model was used to predict temperature dependent behaviors in dispersions containing polymer solutions that display a lower critical solution temperature (LCST). For instance, we predict that capillary induced phase separation may occur below the bulk LCST and that a depletion driven colloidal particle flocculation is replaced by a bridging driven flocculation, at higher temperature. Interestingly, in a temperature interval separating these two regimes, the polymer mediate a particle-particle repulsion, thus stabilizing the dispersion. All these predictions emerge from a model that does not contain temperature dependent interactions.

1.4 DFT for Poisson-Boltzmann theory

DFT can be utilized to obtain ionic mean-field density distributions in an electric double layer system. These distributions are identical to those obtained by solving the Poisson-Boltzmann equation. In a flat surface geometry, with mean-field integrations along x,y directions parellel with the surfaces, the grand potential, Ω, for a 1:1 salt, is given by:

$$\begin{aligned}
\beta\Omega = &\int_0^h n^-(z)\ln[n^-(z)]dz + \int_0^h n^+(z)\ln[n^+(z)]dz \\
&- \int_0^h n^-(z)dz - \int_0^h n^+(z)dz \\
&+\frac{1}{2}\int_0^h\int_0^h n^+(z)n^+(z')\Phi_c(\mid z-z'\mid)dzdz' \\
&+\frac{1}{2}\int_0^h\int_0^h n^-(z)n^-(z')\Phi_c(\mid z-z'\mid)dzdz' \\
&-\int_0^h\int_0^h n^+(z)n^-(z')\Phi_c(\mid z-z'\mid)dzdz' \\
&+\beta\int_0^h n^+(z)V_{ex}^+dz + \beta\int_0^h n^-(z)V_{ex}^-dz \\
&+\int_0^h \Psi_D n^+(z)dz - \int_0^h \Psi_D n^-(z)dz \\
&-\beta\int \mu^+ n^+(z)dz - \beta\int \mu^- n^-(z)dz
\end{aligned} \tag{2.19}$$

where $n^-(z)$ and $n^+(z)$ are the density of cations and anions in the system respectively; $\Phi_c(z) = -2\pi l_B \mid z \mid$, with $l_B = e^2/(kT4\pi\epsilon_0\epsilon_r)$ denoting the Bjerrum length;

V_{ex} is the external filed; Ψ_D is called the Donnan potential, adjusted so as to maintain electroneutrality. The chemical potential for positive and negative ions are defined as:

$$\begin{aligned} \mu^+ &= \mu_{salt} + e\Psi_D \\ \mu^- &= \mu_{salt} - e\Psi_D \end{aligned} \tag{2.20}$$

The grand potential Ω can be minimized as a functional of cation and anion density respectively.

2 Monte Carlo Simulations

Monte Carlo simulations can be utilized to obtain thermodynamic averages, that is in principle are exact, for a given model system. [12]

2.1 Metropolis Algorithm

Metropolis Method

A method in which Monte Carlo simulations sample from Boltzmann distributions was provided by Metropolis *at al.* [12]. It is elegant, simple and applicable to many cases, but it can not provide predictions of dynamical properties.

If $\mathbf{r}^N$ denote the coordinates of N particles, and $\mathcal{U}(\mathbf{r}^N)$ is the potential energy of the system, we can define the configurational integral, Z:

$$Z \equiv \int \exp[-\beta \mathcal{U}(\mathbf{r}^N)] d\mathbf{r}^N \tag{2.21}$$

The Boltzmann probability distribution of finding a system in a configuration around $\mathbf{r}^N$ is given by:

$$p(\mathbf{r}^N) \equiv \frac{\exp[-\beta \mathcal{U}(\mathbf{r}^N)]}{Z} \tag{2.22}$$

However, direct sampling of $p(\mathbf{r}^N)$ is not possible due to the unknown normalization Z. We can then use the Metropolis algorithm. It allows us to sample in an efficient

Boltzmann weighted manner, from the possible configurations, by moving individual particles, and compute averages from microstates.

Consider a system in a configuration $\mathbf{r}^N$ (denoted by o (old)) with a Boltzmann factor $\exp[-\beta\mathcal{U}(o)]$. By adding a small random displacement ($\vec{\Delta}$) to o, a new configuration $\mathbf{r}'^N$ (denoted by n (new)) will be generated, with the new Boltzmann factor $\exp[-\beta\mathcal{U}(n)]$. If the transition probability from configuration o to n is $\pi(o \to n)$, the following condition (Equation 2.23) should be satisfied of equilibrium.

$$p(o)\pi(o \to n) = p(n)\pi(n \to o) \tag{2.23}$$

If the probability of performing a trial move from o to n is $\alpha(o \to n)$, and the probability of accepting a trial move from o to n is $acc((o \to n)$, we have:

$$\pi(o \to n) = \alpha(o \to n) \times acc(o \to n) \tag{2.24}$$

For a symmetric α, with $\alpha(o \to n) = \alpha(n \to o)$, we can obtain:

$$\frac{acc(o \to n)}{acc(n \to o)} = \frac{p(n)}{p(o)} = \exp\{-\beta[\mathcal{U}(n) - \mathcal{U}(o)]\} \tag{2.25}$$

The trial move shall be accepted if:

$$acc(o \to n) = \exp\{-\beta[\mathcal{U}(n) - \mathcal{U}(o)]\} < 1 \tag{2.26}$$

Here, a random number generator is utilized. It can generate a random number (denoted as 'ran') from a uniform distribution in the interval $[0, 1]$. The trial move should be accepted if $ran < acc(o \to n)$, otherwise rejected. However, a good quality random number generator is essential in order to obtain accurate results.

Basic Monte Carlo Algorithm

A basic Metropolis Monte Carlo algorithm is given below:

1. Start from an initial configuration $\mathbf{r}^N$, pick a particle 'p' randomly, and calculate the initial energy $\mathcal{U}(\mathbf{r}_p; \mathbf{r}^{(N-1)}) \equiv \mathcal{U}(o)$.

2. Random displace the particle with $\mathbf{r}'_p = \mathbf{r}_p + \vec{\Delta}$, and calculate the new energy $\mathcal{U}(\mathbf{r}'_p; \mathbf{r}^{(N-1)}) \equiv \mathcal{U}(n)$. Here, $\vec{\Delta}$ is a random displacement.

3. Calculate the energy difference between the two states:

$$\Delta\mathcal{U} = \mathcal{U}(n) - \mathcal{U}(o) \tag{2.27}$$

4. Accept the move if $\Delta\mathcal{U} \leq 0$. If $\Delta\mathcal{U} > 0$, generate a new random number 'ran2', accept the move if $ran2 < \exp(-\beta\Delta\mathcal{U})$.

5. If the move got accepted, update the new configuration and energy, otherwise restore the old configuration, and repeat the steps 2-5 until equilibrium is reached.

Note that, under the assumption of pairwise additive interactions, $\Delta\mathcal{U}$ only requires the calculation of $2(N-1)$ pair interactions.

2.2 Periodic Boundary Conditions

Periodic boundary conditions are adopted in order to mimic the properties of a system in bulk, save computational time, and avoid surface effects.

If a cubic simulation box is used, with periodic boundary conditions, and the box has a length L, it is replicated throughout space to form an infinite lattice. The central box contains N particles, and the coordinates are stored. If a particle moves in the central box, its periodic image in each other boxes will move exactly the same way. And if a particle leaves the box by crossing a boundary, an identical particle will enter from the opposite side. The periodic boundary conditions are illustrated in Figure 2.1.

2.3 Basic Trial Moves

When performing trail moves in Monte Carlo simulations, it is important to sample among all possible configurations. Hence, selecting a reasonable length of the maximum attempted displacement, should be done with some care. A large average displacement will increase the probability for overlap with other particles, and too small displacements will lead to a poor sampling of configurational space. It is common to adjust attempted displacements, so that the average acceptance ratio of trial moves is about $30\% - 50\%$. For hard-sphere systems, the possibility of early rejection, due to overlap, means that it might be preferable to allow a lower acceptance ratio.

Some examples of commonly used trail moves in Monte Carlo simulation are presented here.

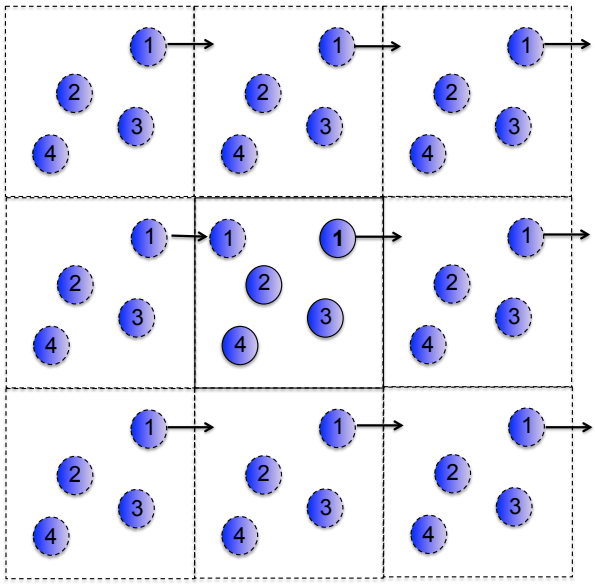

Figure 2.1: Periodic boundary conditions. The thicker solid outline indicates the central box.

Translational Move

Let us first pick a molecule with coordinates x_o, y_o and z_o. Three random values in the interval $[-\Delta/2, \Delta/2]$ can be generated. By adding these values to the old coordinates x_o, y_o and z_o, we can move the molecule translationally to the new coordinates x_n, y_n and z_n.

$$\begin{aligned} x_n &= x_o + \Delta(ran - 0.5) \\ y_n &= y_o + \Delta(ran - 0.5) \\ z_n &= z_o + \Delta(ran - 0.5) \end{aligned} \tag{2.28}$$

Cluster Move

Cluster moves can be adopted in order to make the trial move more efficient in systems containing dense clusters in an otherwise rather dilute environment. Examples include charged colloidal particles, micelles, etc. There are many different kinds of cluster moves. Here we shall describe the simplest one. A cluster is defined as a collection of particles in which each particle is within a chosen cluster radius R_c from at least one other particle in the collection. R_c should be chosen large enough (but

not larger) to contain, on average, essentially all nearest-neighbors surrounding a randomly chosen "tagged" particle. After the other members of the cluster to which the tagged particle belongs have been identified, the entire cluster undergoes a random displacement, i.e. all members are displaced in an identical manner. If the number of members in the cluster changes upon the attempted move, it is rejected. If not, the standard Boltzmann criterion is applied. The former criterion ensures that the condition of microscopic reversibility (Equation 2.23) is fulfilled.

Crank-Shaft Move

When sampling a single chain polymer in Monte Carlo simulation, it is common to perform Crank-Shaft moves, which allow internal rotations within the polymer chain. Pick three linked monomers in a polymer chain randomly, and the middle monomer can rotate around the axis between the other two. This move can be extended to include many monomers, in which case the rotation axis extends longer than between just next-nearest neighbors.

Isobaric Move

If we utilize standard Monte Carlo simulations in the isobaric ensemble, the pressure P, temperature T, and the number of particles N are all fixed parameters, whereas the system volume V is allowed to fluctuate, subject to a standard Metropolis acceptance criterion.

Pivot move

Pivot moves are also devoted to simulations of polymer configurations. A random bond between neighboring monomers is chosen, and a portion of the polymer, on one side of this bond (for instance monomers with a higher index), is randomly rotated around the bond. This move is efficient in dilute conditions, where the risk of overlap with monomers in other polymers, is low.

Chapter 3

Experimental Techniques

Various experimental techniques are utilized in this study. For paper I and II, we used ellipsometry to measure the adsorbed amount of polyelectrolyte. In paper III, osmotic pressure was measured by membrane osmometry. In paper IV, scattering methods were used to investigate the structure of colloidal polymer dispersion.

1 Ellipsometry

Various techniques are available for measuring polyelectrolyte adsorption, such as Dynamic light scattering (DLS) [27, 15] and Photon correlation spectroscopy (PCS) [30], which can be used to measure the hydrodynamic thickness of polyelectrolyte layers adsorbed on colloidal particles. Common techniques for measuring adsorbed mass are Reflectometery [14, 19, 24, 7], X-ray Photoelectron Spectroscopy (XPS) [18], Quartz Crystal Microgravimetry with dissipation monitoring (QCM-D) [7, 26, 13] and Ellipsometry [29, 18, 2, 22, 20].

Ellipsometry is an optical technique based on detecting how polarized light changes upon reflection against interfaces. It is commonly used to characterize adsorption of polymer, proteins or surfactants from aqueous solution. There are three general configurations in ellipsometry techniques, Null Ellipsometer, Static/Dynamic Photometric Ellipsometer and Polarization Modulation Ellipsometers. The latter two have advantages for spectroscopic measurements across a large range of wavelengths, but they are more complicated to use. In this study, Null-Ellipsometry was adopted to measure adsorbed mass of polyelectrolytes on different kinds of surfaces. The advantage is that this technique can monitor the adsorption process *in situ* and generate the results with high accuracy.

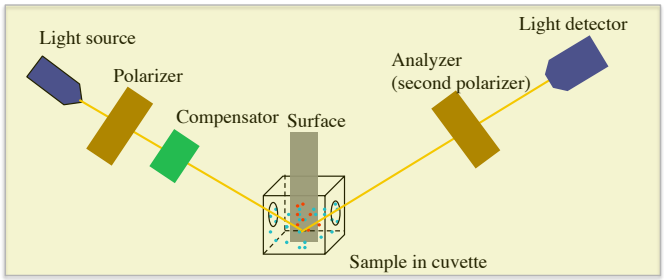

Figure 3.1: Null Ellipsometry experimental set up.

1.1 Null Experimental Set-up

A typical Null Ellipsometry experimental set up is illustrated in Figure 3.1. The light from the Light Source passes through a Polarizer in order to convert the unpolarized light into linearly polarized one. Then the light passes through a Quarter Wave Plate, also called "Compensator", for which the angle of the optical axes is usually set at 45°. This induces a relative phase shift between the two component waves and therefore results in elliptically polarized light. The beam will then pass though the cuvette wall, and the liquid environment before being reflected against the surface. The polarizer is adjusted in such a way that reflected light is linearly polarized and continues thorough an Analyzer. This is a Polarizer used to determine the plane of polarization by finding the settings that produce minimal light intensity as detected by the light detector. The angles of the Polarizer and the Analyzer gives the relative phase shift, Δ, and amplitude change, Ψ, respectively. Although the principles of Null-Ellipsometry were established over hundred years ago, it is still one of the most accurate and robust types of ellipsometers.

1.2 Fundamental Theory of Null Ellipsometry

In Ellipsometry, the polarized light can be decomposed into parallel (p-direction) or perpendicular (s-direction) components of the light waves, relative to the plane of incidence. The interface with the adsorbed layer can be modeled as being composed of a stack of optical isotropic layers. The reflectivity can be described in terms of the complex reflection coefficients along two directions, R_p and R_s. These are a function of the optical properties according to the given optical model. The complex ratio of the total reflection coefficients (R_p/R_s) is directly related to the changes in amplitude (Ψ) and phase shift (Δ) upon reflection [31]:

Table 3.1: Null angles in 4 zone measurements.

	Polarizer	Compensator	Analyzer
Zone 1	$-45^\circ < P_1 < 135^\circ$	-45°	$0^\circ < A_1 < 90^\circ$
Zone 2	$-45^\circ < P_2 < 135^\circ$	45°	$0^\circ < A_2 < 90^\circ$
Zone 3	$-135^\circ < P_3 < 45^\circ$	-45°	$-90^\circ < A_3 < 0^\circ$
Zone 4	$-135^\circ < P_4 < 45^\circ$	45°	$-90^\circ < A_4 < 0^\circ$

$$\frac{R_p}{R_s} = \tan(\Psi)e^{i\Delta} \tag{3.1}$$

Ψ and Δ are quantities measured by the Ellipsometer. So called 4-zone measurements, that is, measurements each of the possible combinations of Polarizer (P), Compensator (C), and Analyzer (A) angles (see Table 3.1) were performed. The readings from each 4 individual measurements of (Δ) and (Ψ) should be equivalent for a perfect optical system and averaging measurements from all four zones compensates for imperfections and misalignment of the system.

From the measurements of Ψ and Δ, the refractive index (n_f) and the thickness (d_f) of the adsorbed film can be determined. These values can then be used to determine the adsorbed mass, Γ, by applying the formula of de Feijter et al.[5]:

$$\Gamma = \frac{(n_f - n_0)d_f}{dn/dc} \tag{3.2}$$

where n_0 is the refractive index of the buffer solution, while dn/dc is the refractive index increment of the adsorbed substance. Both n_0 and dn/dc values can be measured by a Refractometry technique, as described below.

1.3 Optical Models for Surface Layers

Although the Ψ and Δ values can be measured with high accuracy, in order to calculate adsorbed film properties correctly, such as refractive index and thickness, it is vital to choose appropriate optical models. Two optical models, which are called 'four layers model' and 'three layers model', are generally adopted in ellipsometry. These models are illustrated in Figure 3.2.

The optical model employed to determine the optical properties of silica substrate and adsorbed layer properties were based on four layers model: Si-SiO_2-Bulk or Si-SiO_2-Polymer film-Bulk. The optical properties and the thickness of the SiO_2 layer can be determined by measuring the Ψ and Δ values in two different media, *i.e.* air

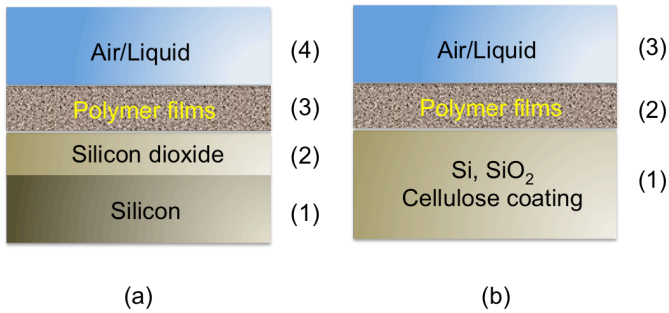

Figure 3.2: Different optical models used in Ellipsometry. (a). Four layers model. (b). Three layers model.

and water, prior to polyelectrolyte adsorption. The Ψ and Δ changes introduced by polyelectrolyte adsorption, can be detected and used to calculate the refractive index and thickness of adsorbed films, from which the adsorbed amount of polymer can be calculated.

Three layers model, *i.e.* Substrate-Bulk, or Substrate-Polymer film-Bulk, were used for the study of the adsorption onto cellulose surfaces, under the assumption that the optical properties of the cellulose layer do not change as polymer adsorb. In this simple model, the optical properties of the substrate were only measured in liquid media. Therefore, the refractive index and the thickness of adsorbed films cannot be resolved independently, but the adsorbed amount is much less sensitive to the optical model applied and can still be calculated accurately.

1.4 Rudolph Ellipsometer

An automated Rudolph Research thin-film null ellipsometer (43603-200E) was used to measure polyelectrolyte adsorption on different kinds of surfaces. All measurements were conducted *in situ* at a wavelength of 401.5 nm with an incident angle of 67.87°, at a temperature of 25°. The liquid cell used for the ellipsometry measurements was a 5 mL trapezoid cuvette made of optical glass with a magnetic stirrer rotating at 300 rpm. After injecting the salt stock solution, Ψ and Δ were recorded as function of time, and when steady state values was obtained, 0.5 mL polymer stock solution was injected to reach the final desired concentration. The adsorption was monitored for at least 1h or until a stable plateau value was established.

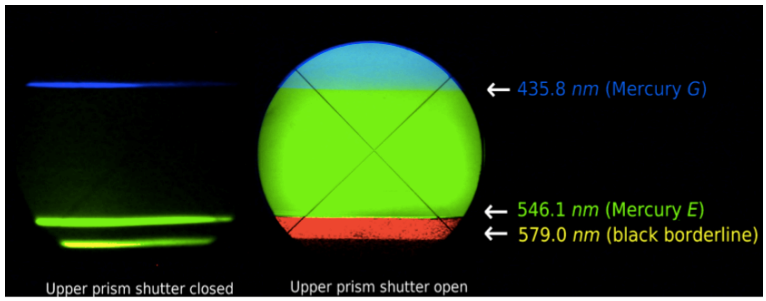

Figure 3.3: Spectral lines as seen through the field telescope of Refractometer with mercury bulb, distilled water as a sample.

2 Refractometry

An Abbe refractometer (Abbe 60/ED) was used to measure the refractive index of salt stock solutions and to determine the refractive index increment of polyelectrolytes at various concentrations, which in turn was used for the calculation of d_n/d_c for determining the adsorbed amount in the elliposmetry measurements. The Abbe refractomter allows us to measure refractive index at three different wavelength, 579.0 nm, 546.1 nm and 435.8 nm. The spectral lines are shown in Figure 3.3. The refractive index at wavelength of 401.5 nm (adopted in Ellipsometery) can be estimated by applying Cauchy's equation:

$$n(\lambda) = A + \frac{B}{\lambda^2} \tag{3.3}$$

3 Membrane Osmometry

Membrane osmometry is a technique that uses a pressure transducer to directly measure the osmotic pressure generated by a solution. It can also be used to measure the number average molecular weight M_n of a polymer sample indirectly, by utilizing virial equations (see Section 5.4) .

The illustration of membrane osmometry is shown in Figure 3.4. The two compartments of membrane osmometry are filled with pure solvent and polymer solution respectively. A semi-permeable membrane separates the two compartments. The pore size of the membrane is such that it allows small solvent molecules to pass though freely, but inhibits the large polymer chains. The net flow of solvent through a semipermeable membrane is driven by a difference in concentration of solute between the two sides of the membrane.

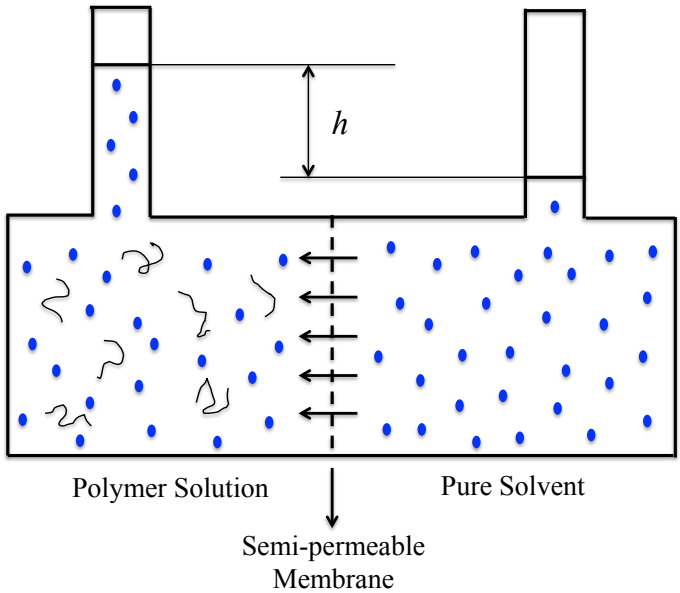

Figure 3.4: The illustration of membrane osmometry technique.

The membrane osmometer used in this study is Osmomat 090 from Gonotec GmbH. It enables the measurement of M_n within the range of 10,000 to 2,000,000 g/mol. It is suitable for both aqueous and organic solvents. The measurement is highly dependent on the membrane that is used. The membrane should have a proper 'cut-off' value, which can efficiently block the polymer chain to pass though the membrane. The polymer should be monodispersed, and highly soluble in the solvent, in order to get accurate results of the M_n.

4 Small-angle Scattering

Small angle scattering (SAS) is a powerful technique for determining the size, shape and orientation of structures in sample. The name 'small-angle' comes from the small deflection angle ($0.1° - 10°$) of the scattered radiation, *e.g.* light, x-rays or neutrons. Most commonly radiation with a single wave length is used. The sample under investigation is exposed to the beam and the intensity of the scattered radiation is analyzed by means of a detector. The obtained scattering intensity versus the scattering vector $q = 4\pi sin(\theta)/\lambda$, where q is the scattering angle and λ is the wavelength, can be used to determine structure and shape of scattering objects in the sample over wide size range, from 10 Å to thousands of Å. This technique can also provide structural information of disordered and inhomogeneous systems. The technique has wide ap-

plications in various areas, such as biological systems, colloidal dispersions and so on. There are two commonly used SAS techniques, small-angle neutron scattering (SANS) and small-angle X-ray scattering (SAXS), which will be describe in more detail below.

Small-angle Neutron Scattering

Small-angle neutron scattering (SANS) is a technique which utilizes elastic neutron scattering to investigate different materials. The particular property of neutrons are scattered by hydrogen very well and that the scattering shows large isotope effect. This allows for so-called contrast matching by using mixtures of H_2O and D_2O as well as specific labeling with deuterium. The wavelength of neutrons is usually from 1-10 Å, which means that it normally is used for objects in the range from 10 Å to several thousands of Å. SANS finds applications in various scientific fields, e.g.soft matter and condensed matter, biology, medical and so on.

Small-angle X-ray Scattering

Small-angle X-ray scattering (SAXS) usually has a higher intensity than neutron scattering, but is much less sensitive for scattering from light elements like hydrogen. X-rays usually have a wavelength from 0.5 - 2 Å , and is therefore often used for objects with size of 50 - 250 Å. X-rays are commonly used to investigate the structural properties of solids, liquids, liquid crystals or gels. Applications are also very broad, including colloids, metals, polymers, proteins, foods and so on.

Chapter 4

Polyelectrolyte Adsorption

Polyelectrolyte adsorption have been studied in paper I and II in this work.

1 Polyelectrolytes

Polyelectolytes are composed of polyions and counterions. Polyions, are polymers carrying positively or/and negatively charged groups. When the polyelectrolytes dissolve in water or other polar solvents, the counterions will be released from the ionic groups to the solution and leave charges on the polymer chain. Polyelectrolytes find many applications in drug delivery, water treatment, paper manufacture, and cosmetics industries and they are also of great scientific interest. Some examples of commonly used polyelectrolytes are listed in Table 4.1.

In this study, two cationic polyelectrolytes, PVNP and PDADMAC are selected to

Table 4.1: Examples of commonly used polyelectrolytes.

Type	Name	
Cationic polyelectrolytes	PDADMAC	Poly(diallyldimethylammonium chloride)
	PVNP	Poly(4-vinyl N-methylpyridinium iodide)
	MPTMAC	Maleimide propyl trimethylammonium chloride
	PEI	Polyethylenimine
	CPAM	Cationic polyacrylamides
	DMAEMA	Poly(Dimethylamino) ethyl methacrylate
Anionic polyelectrolytes	PSS	Polystyrene sulfonate
	PAA	Polyacrylic acid

investigate polyelectrolyte adsorption. Both of the polyelectrolytes are soluble in water to a relatively high concentration, and the charge is not influenced by pH values in the solutions. A short chain version of PVNP (18-mers) is commercially available, and our work includes studies on how polyelectrolyte adsorption is affected by molecular weight.

2 Polyelectrolyte Adsorption

Polyelectrolyte adsorption has generated great interest both theoretically and experimentally, and has therefore been extensively studies in the past. The adsorption of several kinds of polyelectrolytes (both cationic and anionic) and to different types of surfaces, such as charged sulfate latex particles, silica, cellulose fibers and mica, have been studied by using various techniques.[13, 22, 8, 18, 23, 7, 21, 11, 25, 17] However, most of the studies have been focusing on polyions carrying a relatively low charge density. The goal of this study is to understand the process of highly charged cationic polyions adsorbing onto oppositely charged surfaces, in the presence of simple salt. We also investigate the polymer chain length effects on the adsorption, and develop theoretical predictions of these processes, thereby promoting a deeper understanding of the underlying mechanisms of adsorption.

2.1 Polyelectrolytes on Opposite Charged Surfaces

When highly charged polyions adsorb on oppositely charged surfaces, the attractive electrostatic interactions dominate, at least at low ionic strengths. The affinity of the polyions to the surfaces can be so strong that they often overcharge the surfaces, *i.e.*, the surface potential changes sign outside the surface. This overcharging of surfaces can generate long ranged electrostatic double layer free-energy barriers, while at short separation, bridging and ion correlations can mediate a strong attraction. Non-electrostatic contributions, such as hydrophobic interactions, may also contribute to the increased adsorption.

2.2 Effects of pH, Salt Concentration on Adsorption

The pH level, as well as the salt concentration in the polyelectrolyte solutions can affect the adsorption on surfaces. Many previous studies have focused on weakly charged polyelectrolytes with titrating groups [19, 24], where the pH values affect the charge density, and the polymer may become almost neutral even when the surfaces are charged. Thus the electrostatic interaction may then not dominate the polyelec-

trolyte adsorptions. In this work, the charges of the polyelectrolytes are provided by a quartenary ammonium group. Thus the polymer charge is not changing with pH except at high pH. Tris(hydroxymethyl) aminomethane (Tris) buffer was included in the solution to keep the pH at constant (around 9) in the solution.

The addition of a simple salt can not only reduce the electrostatic attractions between positively charged polyions and negatively charged surfaces, but also the repulsion between polyelectrolyte charges. These two counteracting mechanisms can generate a non-monotonic response of the adsorbed amount to the addition of salt. In our systems, we find an adsorption maximum, usually at a salt concentration of about 200 mM. The presence of a limiting plateau value even at very high salt indicates that there are non-electrostatic contributions to the adsorption.

2.3 Molecular Weight Dependence

Effects of molecular weight on polyelectrolyte adsorption have also been considered. Different chain length of polymer can adopt different conformation on surfaces, thus affecting the adsorption behavior. For cellulose surfaces, the short chain polymer has the tendency to penetrate into cellulose layers, and experience a very slow diffusion process. Also, the polydispersity start to play a vital role only when the polymer chain length is very short, typically when the size is below 200 mers.

3 Theoretical Considerations

The equilibrium monomer density profile was generated by using *classical* DFT. With the density profile in our surface-adsorbing solution, the adsorption was calculated as:

$$\Gamma = \int_0^\infty (n_m(z) - n_b)dz \tag{4.1}$$

where n_b is the bulk monomer density and the surface is located at $z = 0$. Experimental adsorption data obtained by Null-ellipsometry are usually reported in units of mass/area, Equation 4.1 provides the excess number of monomers per unit area. By multiplying with the molecular weight of a monomer, direct numerical comparisons can be made with experimental data.

Chapter 5

Polyethylene Oxide in Aqueous Solution

In this work, we present a very simple polymer model of Polyethylene Oxide (PEO) in aqueous solution (see paper VI). This model reproduces several physical properties, such as radii of gyrations, osmotic pressures, and second virial coefficients. This polymer model is also used in our colloidal polymer mixture systems, which will be introduced in the next chapter.

1 Polyethylene Oxide

Polyethylene Oxide (PEO), with a general formula $[(CH_2)_nO]_x$, is one of the most important and widely used polymers in biotechnology, life science, and other industries. It finds applications in drug delivery [1], protein crystallization [4], and so on. PEO is highly soluble in water, and is commercially available in an extraordinarily wide range of molecular weights, ranging from 10^2 to 10^7 g/mol. It is commonly used in fundamental research as well, where its highly solubility, non-toxicity, and well established properties are utilized.

2 Radius of Gyration

The size of a polymer coil can be characterized by its radius of gyration R_g. For a homopolymer, it is defined as:

$$R_g^2 = \frac{\langle \sum_{i=1}^{N_p} \mid \bar{\mathbf{r}}_i - \bar{\mathbf{r}}_{cM} \mid^2 \rangle}{N_p} \tag{5.1}$$

where N_p is the degree of polymerization, $\bar{\mathbf{r}}_i$ denotes the position of the ith segment, and r_{cM} stands for the location of the center mass. The angular brackets denote an average over all possible polymer configurations.

For large N_p, there are scaling relations between R_g and N_p. In a good solvent, polymer chain configurations behave as a self-avoiding random walk, and $R_g \sim N_p^{0.6}$. In a bad solvent, we have $R_g \sim N_p^{0.33}$ instead. For ideal chains in a theta solvent, we have $R_g \sim N_p^{0.5}$ [9].

Theoretically, we can utilize single chain Metropolis Monte Carlo simulations to obtain R_g for our model of PEO, even with M_w of the order of 10^6 g/mol.

3 Osmotic Pressure

When a fluid diffuses through a semipermeable membrane, only solvent molecules are able to pass through the membrane. Osmotic pressure is defined as the pressure which balances the flow of solvent across a semipermeable membrane caused by solute concentration gradients. The formula for calculating the ideal osmotic pressure, Π_{id}, of a solution is:

$$\Pi_{id} = \frac{n}{V} RT = c_b RT \tag{5.2}$$

Where Π is the osmotic pressure, n is number of moles of solute, V is the volume of the solution, R is molar gas constant, and T is the temperature in Kelvin. From the equation we can see that the ideal osmotic pressure is proportional to the molar concentration ($c_b = n/V$) of the solute molecules in solution.

4 Second Virial Coefficient

For a low solute concentration system, we can express the osmotic pressure, Π, in terms of a virial expansion:

$$\frac{\beta\Pi}{c_b} = 1 + B_2 c_b + B_3 c_b^2 + ... \tag{5.3}$$

where B_2 is called second virial coefficient. It measures the pair-interactions in the system. The statistical mechanical expression for B_2, in systems with spherically symmetric interactions, is:

$$B_2 = \int_0^\infty 2\pi r^2 (1 - \exp(-u(r)/k_B T)) dr \tag{5.4}$$

where $u(r)$ is the pair potential (in a polymer solution, it is rather a PMF).

For our PEO solutions, at low polymer concentrations, we expect $\beta\Pi/c_p$ to vary linearly with c_p. The slope is given by B_2, with an unit intercept.

Experimentally, the molecular weight and second virial coefficient can be determined by osmometry measurements. At low polymer concentrations, the virial expansion can be rewritten as:

$$\frac{\beta\Pi}{RTc_b'} = \frac{1}{M_n} + A_2 c_b' + A_3 c_b'^2 + ... \tag{5.5}$$

Here, A_2 is called *osmotic* second virial coefficient, the prime for c_b' indicates a *mass* concentration. The relationship between A_2 and the proper (mass-independent) second virial coefficient B_2 is given as:

$$B_2 = \frac{A_2 M_n^2}{N_A} \tag{5.6}$$

Where N_A is Avogadro's number. By applying linear regression for the osmometry data $\beta\Pi/RTc_b'$ as a function of c_b', we can estimate M_n from the inverse value of the intercept, and A_2 from the gradient value.

5 Theoretical Model

In the Monte Carlo (MC) simulations, we adopted a pearl-necklace model for PEO in an aqueous solution. The model is illustrated in Figure 5.1.

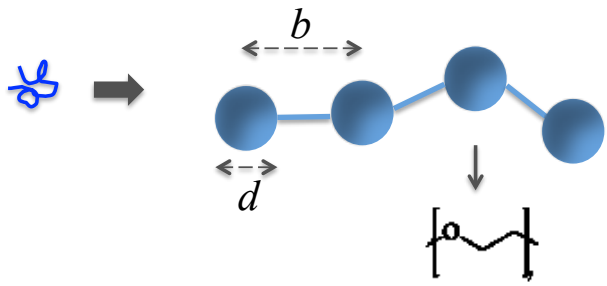

Figure 5.1: Polymer chain model illustration.

In this model, each monomer ($-CH_2 - CH_2 - O$) is represented by a single hard-sphere bead, with a diameter d. These beads are connected by rigid bonds that are orientationally flexible, but with a fixed bond length b. For a given chain length, there are only two adjustable parameters in this model, d and b. These parameters are adjusted for a large range of polymer lengths and concentrations, so that the experimental radii of gyrations and osmotic pressures can be reproduced.

Chapter 6

Colloidal Polymer Dispersion Systems

In this chapter, we consider various colloidal polymer dispersions, which have been previously studied experimentally. We are aiming to construct theoretical models that will generate a deeper understanding of the molecular mechanisms that are responsible for the observed behaviors. (See papers IV, V and VII).

1 Temperature Response of Polymer Mediated Interactions in Particle/Polymer Mixtures

Here, we consider an aqueous solution with uncharged colloidal particles and PEO chains (or similar polymer solutions displaying an LCST), scrutinizing how the system responds to changes of the temperature. This phenomena was recently studied by Feng *et.at.* [10] . They discovered that in a low temperature regime, such systems display a crystalline phase. When increasing temperature, the crystal melts to a homogeneous fluid. Further raising the temperature can cause the system to flocculate again. This is a equilibrium behavior, *i.e.*, after cooling the colloidal polymer mixture to the intermediate temperature regime, it redisperses.

At low temperatures, PEO is relatively hydrophilic, and tends to avoid the particles. When increasing temperature, water becomes less good solvent for PEO, so the solubility of PEO in water decreases. The polymer molecules are then repelled by solvent molecules, and tend to adsorb onto the surfaces. It turns out that (see supporting information of paper IV) polymer mediated interactions between surfaces to which the

monomers have an intermediate affinity, tends to be overall repulsive. We interpret this as a consequence of weakly adsorbed polymers being 'squeezed' before they are forced to leave the slit. This repulsion generates the dispersed phase in the intermediate temperature regime. A further increased temperature will cause hydrophobic PEO to adsorb strongly. This will in turn generate bridging attractions, and a flocculated system.

In this work, we utilize *classic* polymer DFT treatment for Degenerate Systems to investigate temperature dependent polymer mediated interactions in colloid polymer mixtures theoretically. In this model, the monomers are assumed to be in either of two classes of states, A or B, where B is more solvophobic than A. Since the degeneracy of B is higher than A, increasing the temperature will cause the population of solvophobic monomers to increase. If the colloidal particles are solvophobic, this model can then display the same qualitative temperature response as was observed by Feng *et.at.*. This is achieved without any assumptions of temperature-dependent interactions.

We use the same polymer model was described in the last chapter for PEO, *i.e.* N freely jointed hard sphere beads, connected by rigid bonds. The number of beads is 1600, representing 1600-mer PEO [1]. The bond length b was chosen to reproduce experimentally observed R_g. The hard sphere diameter d was 3.1 Å, *i.e.* solvent molecules and monomers are assumed to have the same size. The potential of mean force between colloidal particles was generated via the Derjaguin Approximation, since the particle size (radius was $2-4\mu m$) was much larger than monomers ($R_g = 40nm$). The spherical particles were thus modeled as two infinitely large planar surfaces, immersed in a polymer solution.

2 Temperature Induced Gelation in Colloidal Dispersions with Grafted Polymers

Polymers can be grafted onto colloidal particles, in order to stabilize the colloidal dispersion. However, many polymer-solvent systems display a LCST, i.e. they demix upon heating. A theta temperature (T_θ) for this system is defined as the temperature where one finds an LCST for solutions with very long polymers. When the temperature apporaches T_θ, colloidal dispersions containing particles with grafted chains may flocculate or form a gel. This phenomenon has been previously studied experimentally by Shay *et.at.* [28]. Surprisingly though, they obsearved gelation at temperatures far below T_θ.

In this work, we used the previously introduced polymer model for PEO, and *classic*

[1] The results are quite insensitive to the degree of polymerization.

polymer DFT treatment for degenerate systems to investigate these polymer-induced interactions.

3 Charged Colloidal Particles and Non-adsorbing Polymers

This system contained charged polystyrene particles with water soluble PEO chains. The particles were coated with a surfactant layer, in order to effectively stabilize the particles against van der Waals (vdW) attractions. Surface charges on the colloidal particles were introduced by addition of charged co-monomers, and the range of the electrostatic double-layer repulsion was regulated by monovalent salt. Two salt concentrations, 50 mM and 1.5 mM were considered, in order to scrutinize cases of fully screened and intermediate-ranged electrostatic repulsion. The non-adsorbing PEO polymer, acting as depleting agent, was added into the system. The colloidal particles will form gel above a certain polymer concentration due to depletion attractions. This system has been previously investigated experimentally by scattering methods [34, 33, 32]. Our aim here is to construct a coarse-grained model, to quantitatively compare the predicted structure factors with corresponding experimental data.

The polymer model for PEO that we adopt here was introduced in the previous chapter. We use *classical* polymer DFT to predict the polymer-induced depletion attraction. This theory will qualitatively capture the correlation length drop that results from an increased concentration. The DFT treatment for full PB is used to predict the long-ranged electrostatic repulsion, which can increase the accuracy at short range compared with using Screened Coulomb (SC) potentials. The particles have a hard sphere radius of about 600 Å, which is more than one order of magnitude lager than the R_g of the polymers (47 Å). This allows us to utilize the Derjaguin Approximation (DA) for generating the potential of mean force between colloidal particles. The particle surfaces were modeled as infinite parallel flat walls. Canonical Metropolis Monte Carlo simulations were used to generate radial distribution functions, $g(r)$, which were Fourier transformed to obtain the corresponding structure factors. These can be directly compared with experimental data. Note that the surface charge of particles is an experimental unknown parameter. We defined this value so that the experimental and theoretical gel points were obtained at equal polymer concentrations.

Chapter 7

Main Results of the Research Papers

In this chapter, we summarize our results for all the articles included in this thesis.

Paper I

Polyelectrolytes Adsorption on Solid Surfaces: Theoretical Predictions and Experimental Measurements

Two different types of highly charged cationic polyelectrolytes, PVNP and PDADMAC, have been used to explore the adsorption onto oppositely charged silica surfaces. How the adsorption varies with concentration of simple salt has been particularly considered. Theoretical predictions from *classical* DFT for polyelectrolytes were compared with corresponding experimental data, which was obtained by ellipsometery measurements (Figure 7.1). Figure 7.1 shows that for both polyelectrolytes, when increasing salt concentration, the adsorption increases first, but reaches a maximum value, after which it drops but appears to approach a plateau value at very high salt levels. The latter observation indicats that the adsorption is not entirely of electrostatic origin. By including a non-electrostatic adsorption potential as well as an approximation of ion correlation effects, in our model, we obtained excellent agreement between experimental data and theoretical predictions.

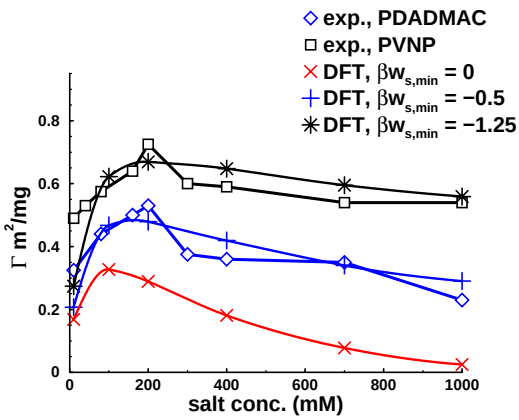

Figure 7.1: Comparing the net adsorption of PDADMAC and PVNP as measured by ellipsometry and calculated by polymer DFT, respectively. $w_{s,min}$ measures the strength of a non-electrostatic adsorption potential.

Paper II

Theoretical and Experimental Investigation of Polyelectrolyte Adsorption Dependence on Molecular Weight

In this work, we used a highly charged cationic polyelectrolyte, PVNP, with two different chain lengths (degree of polymerizations), to investigate the polyelectrolyte adsorption dependence on molecular weight. The experimental results obtained by ellipsometry have been compared with theoretical predictions by polymer DFT. We used two different models. In model I, the electrostatic contributions, which act only on charged beads, are taken from the standard Guy-Chapman model. This is the same model as we adopted in paper I. In model II, the electrostatic contributions between charged beads are described by Screened Coulomb interactions. Furthermore, in model I, 'PVNP' and 'PDADMAC' are identified by their respective non-electrostatic adsorption strengths. In model II this adsorption strength is the same for the two polymers, and we instead discriminate betwen the polymers by the effective monomer size. Comparisons between theory and experiments are shown in Figure 7.2. Both models give good agreements with experimental data. At every salt concentration, the adsorbed amount is higher for the longer polymer.

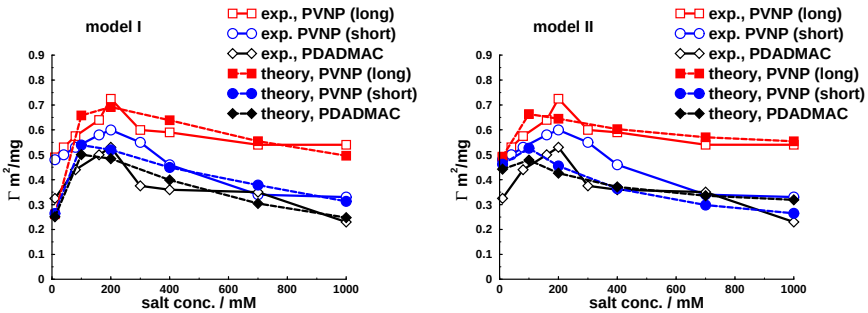

Figure 7.2: Experimental measurements and theoretical predictions on adsorbed amount of different types of polyelectrolytes at a silica surface, as a function of salt concentration. Two different polymer models have been utilized.

The adsorption of PVNP on cellulose surfaces has also been tested experimentally. We see in Figure 7.3, the adsorption on cellulose surfaces is much more pronounced than on silica surfaces. This is possibly due to the cellulose surfaces being rougher than silica, i.e., the actual surface area for the cellulose substrate might be substantially larger than for the silica surface.

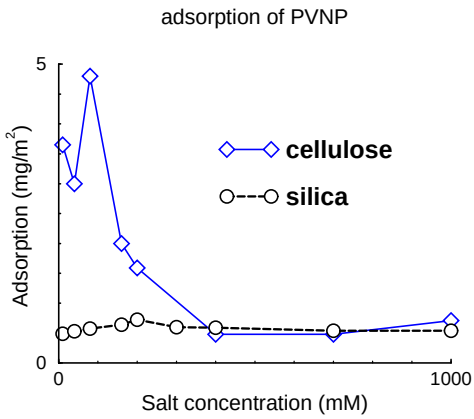

Figure 7.3: Experimental measurements of PVNP on silica and cellulose surface as a function of salt concentration.

Paper III

Fluid-Fluid Transitions at Bulk Supercritical Conditions

We predict the existence of capillary-induced phase separations (CIPS) in pores under supercritical bulk conditions, using three different polymer solvent mixture models. The theoretical method is *classical* DFT. All fluid mixture models may undergo CIPS

in narrow pores, even under conditions where there is only a single phase in the bulk. Examples of phase diagrams for pores of different widths is displayed in Figure 7.6. When the slit width becomes more narrow, demixing progresses more deeply into the supercritical regime, as shown in Figure 7.4. The capillary critical temperature is more than 10% below the bulk LCST, for the narrow pore.

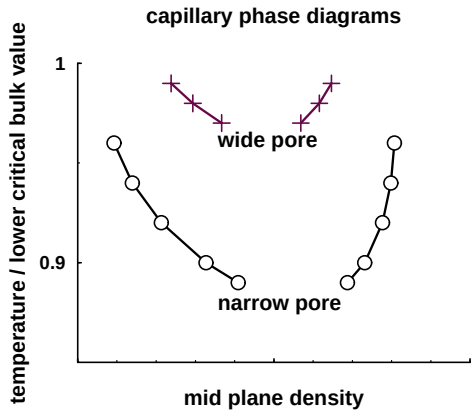

Figure 7.4: Phase diagrams for pores of different widths.

Paper IV

Non-monotonic Temperature Response of Polymer Mediated Interactions

Here we constructed a polymer + particle dispersion model, used *classical* DFT for degenerate systems, to investigate the non-monotonic temperature response of polymer mediated interactions in colloidal polymer systems that display a LCST. Our model does not rely upon any temperature-dependent interactions, and all possible polymer configurations are accounted for, subject to a mean-field Boltzmann weight. We found out that the interactions between colloids mediated by the polymers follows the trend: attraction $\Rightarrow$ repulsion (or vanishing interaction) $\Rightarrow$ attraction as the surface affinity toward monomers proceeds from repulsive to attractive (Figure 7.5). This is in qualitative agreement with experimental findings by Feng *et.al.* [10], *i.e.* colloidal system follows the trend flocculated $\Rightarrow$ homogeneous dispersion $\Rightarrow$ flocculated upon increasing temperature.

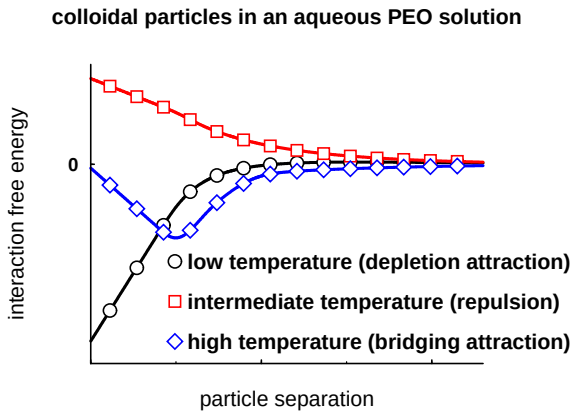

Figure 7.5: Net interaction free energy versus particle separation, at various temperatures.

Paper V

Theoretical Predictions of Temperature-induced Gelation in Aqueous Dispersions Containing PEO-grafted Particles

We studied a model for polystyrene particles with grafted PEO chains. DFT for degenerate system was used in this work. We found out that when the PEO polymers are grafted onto polystyrene particles, bridging can occur at temperatures below the LCST. The occurrence of these attractive interactions are able to cause gelation of the polystyrene (PS) particles at temperatures well below LCST. Shay et al. also found that the gelation temperature was reduced for lower grafting densities. They suggested that dispersion interactions are the main driving force for gelation. In agreement with experimental findings by Shay et al., we locate gelation at temperatures considerably below T_θ, and far below the LCST for such chain lengths. This gelation occurs also without any dispersion (van der Waals) interactions between the PS particles. Interestingly, the polymer-induced interaction free energy displays a non-monotonic dependence on the grafting density. At high grafting densities, bridging attractions between grafted layers take place (considerably below T_θ). At low grafting densities (Figure 7.6), on the other hand, the polymers are able to bridge across to the other particle surface. Shay et al. conducted their experiments at very low ionic strength, using de-ionized water as a solvent. We demonstrate that even minute amounts of adsorbed charge on the surface of the particles, can lead to dramatic changes of the gelation temperature, especially at high grafting densities. Another interesting prediction is the existence of elongated (chain-like) equilibrium structures, at low particle concentrations.

Figure 7.6: Simulation snapshots of structures obtained at low volume fractions (1%). in systems in which the grafted particles also carry a weak charge, in solutions containing 0.01 mM monovalent salt.

Paper VI

A Simple and Versatile Implicit Solvent Model for Polyethylene Glycol in Aqueous Solution at Room Temperature

We developed a very simple polymer model to accurately reproduce experimental data on osmotic pressure and radius of gyration. Figure 7.7 shows that the simulated osmotic pressures display have a good agreement with osmometry measurements as well as with Cohen's equation of state (EOS) [3].

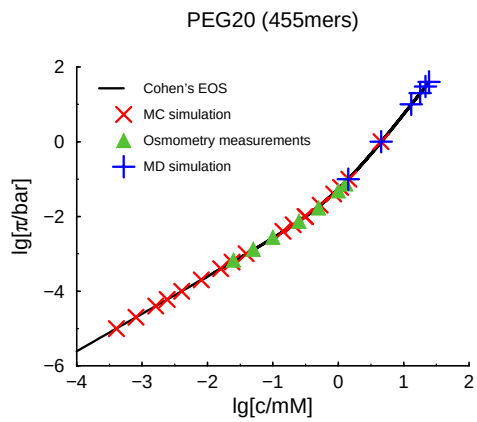

Figure 7.7: Osmotic pressure as a function of polymer concentration for PEG20 (455 mers) from MC and MD simulations, Osmometry measurements, and Cohen's EOS.

The comparison of simulated radii of gyrations with an empirical expression fitted to a range of experimental data, is shown in Figure 7.8.

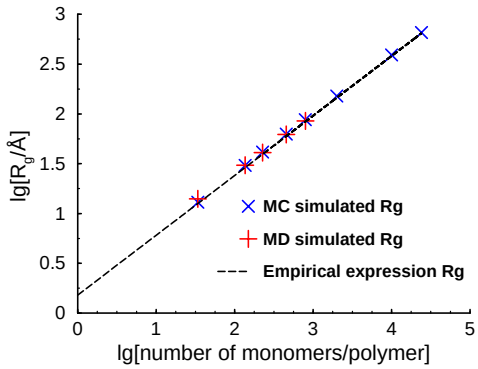

Figure 7.8: Simulated and empirical values of radius of gyration of a single PEG chain with different chain lengths.

We also evaluated the second virial coefficient, and its dependence on the polymer chain length. The results are provided in Figure 7.9. The observed slope is in reasonable agreement with the value 1.76 that is expected from scaling theory. Note that Polyethylene Glycol (PEG) and Polyethylene Oxide (PEO) are synonymous.

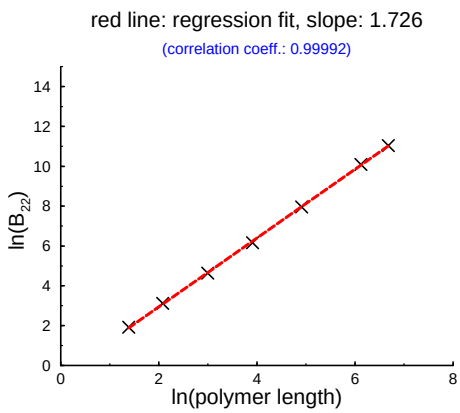

Figure 7.9: MC simulation results of second virial coefficient as a function of polymer length.

Paper VII

Theoretical Predictions of Structure in Dispersions Containing Charged Colloidal Particles and Non-adsorbing Polymers

In this work, we developed a theoretical model to describe structural effects on systems containing charged colloidal particles and non-adsorbing PEO polymers. *Classical* polymer DFT is used to calculate the polymer induced depletion attractions, and full PB is utilized for electrostatic repulsion. We have demonstrated that the DFT is able to accurately capture the correlation length drop that results from an increase if the polymer concentration. Full PB has the advantage, compared with its linearized version, that it is accurate (under these circumstances) also at short range, which is a regime that is crucial to the development of a gel. The comparison between theoretical predictions and corresponding experimental data for the structure factor at different salt concentrations is shown in Figure 7.10. A satisfactory agreement is found for a range of polymer concentrations.

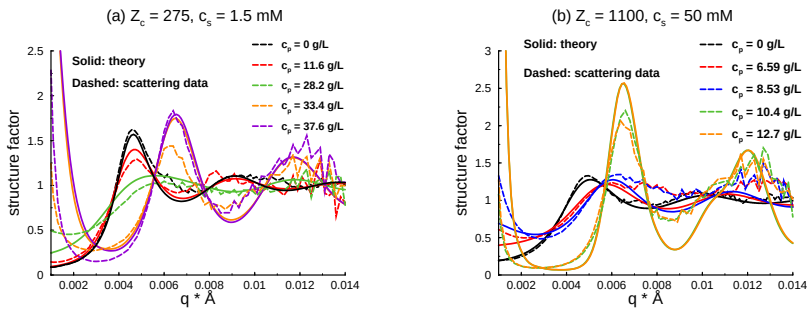

Figure 7.10: Theoretical and SANS data for structure factors of colloidal particles and PEO mixtures. (a). Salt concentration: 1.5mM. (b). Salt concentration: 50mM.

References

[1] Monica L. Adams, Afsaneh Lavasanifar, and Glen S. Kwon. Amphiphilic block copolymers for drug delivery. *Journal of Pharmaceutical Sciences*, 92(7):1343–1355, 2003.

[2] Daniel Angelescu, Tommy Nylander, Lennart Piculell, Per Linse, Björn Lindman, Juergen Tropsch, and Juergen Detering. Adsorption of branched-linear polyethyleneimine-ethylene oxide conjugate on hydrophilic silica investigated by ellipsometry and monte carlo simulations. 27(16):9961–9971, 2011.

[3] J. A. Cohen, R. Podgornik, P. L. Hansen, and V. A. Parsegian. A phenomenological one-parameter equation of state for osmotic pressures of peg and other neutral flexible polymers in good solvents. *The Journal of Physical Chemistry B*, 113(12):3709–3714, 2009. PMID: 19265418.

[4] R. Cudney, S. Patel, K. Weisgraber, Y. Newhouse, and A. McPherson. Screening and optimization strategies for macromolecular crystal growth. *Acta Crystallographica Section D*, 50(4):414–423, Jul 1994.

[5] J. A. De Feijter, J. Benjamins, and F. A. Veer. Ellipsometry as a tool to study the adsorption behavior of synthetic and biopolymers at the air water interface. *Biopolymers*, 17(7):1759–1772, 1978.

[6] J. R. Ebdon. Introduction to polymers (second edition). *Polymer International*, 27(2):207–208, 1992.

[7] Lars-Erik Enarsson and Lars Wågberg. Adsorption kinetics of cationic polyelectrolytes studied with stagnation point adsorption reflectometry and quart z crystal microgravimetry. *Langmuir*, 24(14):7329–7337, 2008. PMID: 18553950.

[8] Lars-Erik Enarsson and Lars Wågberg. Polyelectrolyte adsorption on thin cellulose films studied with reflectometry and quartz crystal microgravimetry with dissipation. *Biomacromolecules*, 10(1):134–141, 2009. PMID: 19053297.

[9] F. A. Evans and H. Wennerström. *The colloidal domain: where Physics, Chemistry, Biology and Technology meet*. VCH Publishers, New York, 1994.

[10] Lang Feng, Bezia Laderman, Stefano Sacanna, and Paul Chaikin. Re-entrant solidification in polymer–colloid mixtures as a consequence of competing entropic and enthalpic attractions. *Nat Mater*, 14(1):61, 2015.

[11] Laurent Feuz, Frans A. M. Leermakers, Marcus Textor, and Oleg Borisov. Adsorption of molecular brushes with polyelectrolyte backbones onto oppositely charged surfaces: A self-consistent field theory. *Langmuir*, 24(14):7232–7244, 2008. PMID: 18558731.

[12] Daan Frenkel and Berend Smit. Chapter 3 - monte carlo simulations. In Daan Frenkel and Berend Smit, editors, *Understanding Molecular Simulation (Second Edition)*, pages 23 – 61. Academic Press, San Diego, second edition edition, 2002.

[13] Akhilesh Garg, James R. Heflin, Harry W. Gibson, and Richey M. Davis. Study of film structure and adsorption kinetics of polyelectrolyte multilayer films: Effect of ph and polymer concentration. *Langmuir*, 24(19):10887–10894, 2008. PMID: 18785708.

[14] Nanthiya Hansupalak and Maria M. Santore. Sharp polyelectrolyte adsorption cutoff induced by a monovalent salt. *Langmuir*, 19, 2003.

[15] J. Hierrezuelo, I. Szilagyi, A. Vaccaro, and M. Borkovec. Probing nanometer-thick polyelectrolyte layers adsorbed on oppositely charged particles by dynamic light scattering. *Macromol.*, 43:9108, 2010.

[16] Gunnar Karlström. A new model for upper and lower critical solution temperatures in poly(ethylene oxide) solutions. *The Journal of Physical Chemistry*, 89(23):4962–4964, 1985.

[17] F. A. M. Leermakers, J. Bergsma, and J. van der Gucht. Hybrid monte carlo self-consistent field approach to model a thin layer of a polyelectrolyte gel near an adsorbing surface. *The Journal of Physical Chemistry A*, 116(25):6574–6581, 2012. PMID: 22397698.

[18] R. Mészáros, I. Varga, and T Gilányi. The effect of salt concentration on adsorption of low-charge-density polyelectrolytes and interactions between polyelectrolyte-coated surfaces. *Langmuir*, 20:5026–5029, 2004.

[19] R. Meszaros, L. Thompson, M. Bos, and P. de Groot. Adsorption and electrokinetic properties of polyethylenimine on silica surfaces. *Langmuir*, 18:6164, 2002.

[20] Andreas Mohr, Tommy Nylander, Lennart Piculell, Björn Lindman, Volodymyr Boyko, Frank Wilko Bartels, Yaqian Liu, and Vandana Kurkal-Siebert. Mixtures of cationic copolymers and oppositely charged surfactants: Effect of polymer charge density and ionic strength on the adsorption behavior at the silica aqueous interface. *ACS Applied Materials and Interfaces*, 4(3):1500–1511, 2012. PMID: 22301772.

[21] M. Muthukumar. Adsorption of a polyelectrolyte chain to a charged surface. *The Journal of Chemical Physics*, 86(12):7230–7235, 1987.

[22] Lars Oedberg, Sussan Sandberg, Stefan Welin-Klintstroem, and Hans Arwin. Thickness of adsorbed layers of high molecular weight polyelectrolytes studied by ellipsometry. *Langmuir*, 11(7):2621–2625, 1995.

[23] Roland Rehmet and Erwin Killmann. Adsorption of cationic poly(diallyl-dimethyl-ammoniumchloride), poly(diallyl-dimethyl-ammoniumchloride-co-n-methyl-n-vinylactamide) and poly(n-methyl-n-vinyl-acetamide) on polystyrene latex. *Colloids and Surfaces A: Physicochemical and Engineering Aspects*, 149(1–3):323–328, 4 1999.

[24] Oj. Rojas, Pm. Claesson, D. Muller, and Rd. Neuman. Adsorption of poly(ethyleneimine) on silica surfaces effect of ph on the reversibility of adsorption. *Journal of colloid and interface science*, 205:77–88, 1998.

[25] O. V. Rud, A. A. Mercurieva, F. A. M. Leermakers, and T. M. Birshtein. Collapse of polyelectrolyte star. theory and modeling. *Macromolecules*, 45(4):2145–2160, 2012.

[26] T. Saarinen, M. Österberg, and J. Laine. Properties of cationic polyelectrolyte layers adsorbed on silica and cellulose surfaces studied by qcm-d-effect of polyelectrolyte charge density and molecular weight. *J. Coll. Disp. Sci.*, 30:969, 2009.

[27] E. Seyrek, J. Hierrezuelo, A. J. Sadeghpour, I. Szilagyi, and M. Borkovec. Molecular mass dependence of adsorbed amount and hydrodynamic thickness of polyelectrolyte layers. *Phys. Chem. Chem. Phys.*, 13:12716, 2011.

[28] Jennifer S. Shay, Srinivasa R. Raghavan, and Saad A. Khan. Thermoreversible gelation in aqueous dispersions of colloidal particles bearing grafted poly(ethylene oxide) chains. *Journal of Rheology*, 45(4):913–927, 2001.

[29] V. Shubin and P. Linse. Effect of electrolytes on adsorption of cationic polyacrylamide on silica: Ellipsometric study and theoretical modeling. *J. Phys. Chem.*, 99:1285, 1995.

[30] M. A. Cohen Stuart, F. H. W. H. Waajen, T. Cosgrove, B. Vincent, and T. L. Crowley. Hydrodynamic thickness of adsorbed polymer layers. *Macromolecules*, 17(9):1825–1830, 1984.

[31] HARLAND G. TOMPKINS. Chapter 1 - theoretical aspects. In Harland G. Tompkins, editor, *A User's Guide to Ellipsometry*, pages 1 – 18. Academic Press, San Diego, 1993.

[32] Kitty van Gruijthuijsen, Wim G. Bouwman, Peter Schurtenberger, and Anna Stradner. Direct comparison of sesans and saxs to measure colloidal interactions. *EPL (Europhysics Letters)*, 106(2):28002, 2014.

[33] Kitty van Gruijthuijsen, Marc Obiols-Rabasa, Marco Heinen, Gerhard Nägele, and Anna Stradner. Sterically stabilized colloids with tunable repulsions. *Langmuir*, 29(36):11199–11207, 2013. PMID: 23937718.

[34] Kitty van Gruijthuijsen, Remco Tuinier, Joseph M. Brader, and Anna Stradner. Phase behaviour of colloids with short-range repulsions plus nonadsorbing polymer chains. *Soft Matter*, 9:9977–9982, 2013.

[35] Clifford E. Woodward. Density functional theory for inhomogeneous polymer solutions. *J. Chem. Phys.*, 94:3183, 1991.

Scientific Publications

Author Contributions

Paper I: Polyelectrolyte adsorption on solid surfaces: theoretical predictions and experimental measurements.

I designed and performed the experiments, analyzed the experimenal data, and wrote the experimental part of the manuscript.

Paper II: Theoretical and experimental investigations of molecular weight dependence on polyelectrolytes adsorption

I designed and performed the experiments, analyzed the experimenal data, and wrote the experimental part of the manuscript.

Paper III: Fluid-fluid transitions at bulk supercritical conditions.

I ran the DFT calculations, analyzed the data, and participated in writing manuscript.

Paper IV: Non-monotonic temperature response of polymer mediated interactions.

I ran the DFT calculations, analyzed the data, and participated in writing manuscript.

Paper v: Theoretical Predictions of Temperature-Induced Gelation in Aqueous Dispersions Containing PEO-Grafted Particles

I ran the DFT calculations, analyzed the data, and participated in writing manuscript.

Paper vi: A simple and versatile implicit solvent model for Polyethylene Glycol in aqueous solution at room temperature.

I ran the MC simulations and DFT calculations, built my own single chain MC code, and wrote the first draft of the manuscript.

Paper vii: Theoretical predictions of structures in dispersions containing charged colloidal particles and non-adsorbing polymers..

I ran the MC simulations and DFT calculations, and wrote my own DFT (Poisson-Boltzmann + polymer) as well as MC codes (for the polymer DFT, I borrowed excess free energy (GFD) routines from an existing code), and wrote the first draft of the manuscript.